

Chapter 2

Single-Molecule Imaging of LacI Diffusing Along Nonspecific DNA

Y.M. Wang and R.H. Austin

2.1 Introduction

Transcription factors, restriction enzymes, and RNA polymerases are proteins that function by binding to their specific target sites on DNA [1, 2]. The DNA targets for these proteins are typically a few tens of base pairs long, while the chromosomes contain over a million base pairs of DNA (*E. coli*, for example, has 4.6 million base pairs); therefore, before reaching their targets, it is inevitable that DNA-binding proteins encounter nonspecific DNA first. In this process, protein–nonspecific-DNA binding does occur (although with weaker affinity than DNA target binding [3]) and this interaction affects the specific-DNA targeting rate of the protein. In order to regulate the targeting rate of DNA-binding proteins, which is an important step for gene expression regulations, the mechanisms of protein interaction with nonspecific DNA must be elucidated.

The notion that nonspecific DNA influences the targeting rate of DNA-binding proteins gained renewed credence when faster-than-diffusion target binding of LacI (Lactose repressor protein) was observed in 1970. LacI binds to its lactose operator target (*lacO*) 100 times faster than allowed by the 3D diffusion limit [4]. This faster-than-diffusion binding was explained by the facilitated-diffusion model, in which a DNA-binding protein interacts with nonspecific DNA before reaching its target [5–18].

A facilitated-diffusion process is composed of three main types of protein's motion around DNA: sliding, where the protein translocates (or slides) along non-specific DNA base pairs without losing contact (Fig. 2.1, green arrows); hopping, where the protein dissociates from DNA briefly, performing free 3D diffusion, and lands back on DNA at a location that is shorter than the DNA's persistence length away from the dissociation site (Fig. 2.1, black arrows); and jumping, where the protein's DNA landing location is not correlated to the dissociation site [15].

Y.M. Wang (✉)

Department of Physics, Washington University in St. Louis, Saint Louis, MO, 63130

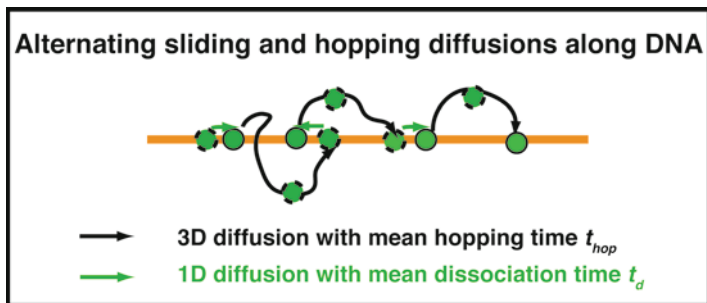


Fig. 2.1 Sliding and hopping diffusions of a protein (green) on an elongated DNA molecule (orange). Typical experimentally observed seconds-long protein trajectories on DNA should have many sliding and hopping alternations convolved. The mean 1D sliding time (or nonspecific DNA dissociation time) and 3D hopping time are t_d and t_{hop} , respectively

Figure 2.1 shows that for the typical elongated DNA geometry used in single-molecule fluorescence imaging experiments, a protein performs a series of alternating sliding and hopping motions along DNA. In a cell, the targeting process can be further complicated by road blocks of other bound proteins on DNA and different configurations of the chromosomal DNA due to confinement [19–21]. In this chapter, we focus on sliding and hopping diffusions of proteins on DNA since most single-molecule fluorescence imaging experiments use low concentrations of elongated DNA molecules for which jumping and in vivo effects are absent.

In order to calculate the effects of facilitated diffusion on the targeting rate of proteins, all three components of the facilitated-diffusion process as well as the switching kinetics among the different components should be quantified. Hopping and jumping motions are 3D Brownian motions of proteins in water, and the dynamics of 3D Brownian motions are relatively well understood, in contrast to sliding. For the sliding motion, two major issues await investigation due to limitations of current single-particle-tracking techniques: (1) The translocation (or sliding) mechanism of a protein on DNA sequences is not fully understood. There are two main translocation models: one is the DNA-sequence-independent model, where proteins are insensitive to DNA sequences and perform Brownian diffusion on DNA; the other is the DNA-sequence-dependent model, where the sliding diffusion characteristics are time dependent – anomalous subdiffusion in short millisecond timescales and Brownian diffusion in long second timescales [22]. (2) The mean sliding time and hopping time, or the protein-nonspecific-DNA dissociation rate constant (or nonspecific-DNA dissociation time, or sliding time) t_d and 3D hopping time t_{hop} , respectively, are not precisely known. Uncertainties in these parameters will decrease the accuracy of protein targeting rate calculations.

This chapter emphasizes studies of the sliding component of facilitated diffusion (and along with it the sliding–hopping alternation kinetics) using single-molecule fluorescence imaging methods. LacI is used as a model protein, and DNA molecules are elongated along fused-silica surfaces. The elongated DNA configuration offers a simple platform for revealing the dynamics of protein translocation on DNA base

pairs during sliding, which is essential for understanding facilitated diffusion for any DNA configurations in cells. Why use the single molecule method? Conventional bulk measurements have been very powerful in validating and characterizing facilitated diffusion [4, 8, 10, 13, 16, 18, 23–25]; however, in order to characterize the sliding mechanisms of proteins on DNA, the motion of proteins on DNA has to be tracked. Thus, single-molecule imaging is an ideal candidate for these studies.

This chapter is divided into three parts: First, we present our initial study of LacI diffusion on nonspecific DNA in the timescale of seconds performed in 2006. Prior to this study, two articles had reported on the direct imaging of proteins diffusion on DNA. One was by Nobuo Shimamoto [12] and the other was by Yoshie Harada et al. [26]. In the first article, it is not clear whether the proteins interact with a single DNA molecule, or an array of DNA molecules; and in the second article the diffusion characteristics are not analyzed. Our study addresses both issues. Next, we discuss the limitations of current instrumentation and the single-molecule point spread function (PSF) centroid tracking method for technically demanding studies of molecule sliding, which require millisecond temporal resolution and nanometer spatial resolution. We introduce our new single-molecule image deconvolution (SMID) method, which meets these technical demands and we present the results of our preliminary application of SMID to LacI sliding studies. Using the SMID method, sliding and sliding–hopping alternation characteristics can be extracted from single protein-diffusing-on-DNA images in millisecond and sub-millisecond exposure times; and thus the SMID method increases the temporal resolution of single-particle tracking by at least 100-fold from ≈ 300 ms to milliseconds and sub-milliseconds (Sect. 2.4.1). Lastly, we outline additional studies necessary for single-molecule investigations of protein sliding on DNA using SMID.

2.2 Early LacI Diffusion Experiments in the Timescale of Seconds

2.2.1 *Facilitated Target Association Rate Calculation Assuming Brownian Sliding*

In this section, we discuss our single-molecule imaging studies of one-dimensional diffusion of LacI repressor proteins along elongated DNA in the timescale of seconds. Our analysis of the LacI transcription factors' diffusion yielded four main results: (1) LacI diffuses along nonspecific DNA in the form of 1D Brownian motion, (2) the observed 1D diffusion coefficients D_1 vary over an unexpectedly large range, from $2.3 \times 10^{-12} \text{ cm}^2/\text{s}$ to $1.3 \times 10^{-9} \text{ cm}^2/\text{s}$, (3) the lengths of DNA covered by these 1D diffusions vary from 120 nm to 2920 nm, and (4) assuming that the LacI sliding is Brownian for all timescales, the mean values of D_1 and the diffusional lengths indeed predict a LacI target binding rate 90 times faster than the 3D diffusion limit.

The expected association rate $k_{a(3D)}$ by which DNA-binding proteins find their specific target sequences on double-stranded DNA in a random 3D search is $4\pi D_3 l_{seq}$ per unit protein concentration, where l_{seq} is the effective DNA target length, and $D_3 = k_B T / 3\pi\eta a = 9 \times 10^{-7} \text{ cm}^2/\text{s}$ is the 3D diffusion coefficient of the protein in solution [4, 15, 27], where k_B is the Boltzmann constant, T is the temperature, η is the viscosity of the solvent, and $a \approx 5 \text{ nm}$ is the typical diameter of the protein. With $l_{seq} \approx 3 \text{ bp}$ (or 1 nm), the protein–DNA association rate $k_{a(3D)}$ should be $10^8/\text{M}\cdot\text{s}$. The original in vitro study on LacI-*lacO* binding by Riggs et al. was with 45.5 kbp DNA of $15.5 \mu\text{m}$ in length, and the *lacO* association rate $k_{a(Exp)}$ was measured to be $10^{10}/\text{M}\cdot\text{s}$, 100 times higher than the diffusion limit of $k_{a(3D)} \approx 10^8/\text{M}\cdot\text{s}$ [4] (the $10^{10}/\text{M}\cdot\text{s}$ binding rate was also reported in [13, 15, 28]).

It has been proposed that such high rates can be achieved if the protein undergoes a facilitated-diffusion process in which the protein performs a combination of 1D diffusion along the DNA and 3D diffusion in solution. In this model, the key to faster targeting lies with the nonspecific DNA sequences that flank the target site. By 3D diffusion, a protein most likely will run into a segment of nonspecific DNA first. After nonspecific binding, the protein will diffuse along the DNA for a certain time and eventually dissociate. By doing so, the effective concentration of protein near the DNA increases, and thus the targeting rate should change. This facilitated-diffusion modified protein-target association rate k_a per protein concentration has been derived by Halford and Marko [15]:

$$k_a = \left(\frac{1}{D_3 l_d} + \frac{L l_d c}{D_1} \right)^{-1} = k_{a,3D} \left(\frac{l_{seq}}{l_d} + \frac{D_3}{D_1} l_{seq} L l_d c \right)^{-1}, \quad (2.1)$$

where D_1 is the 1D diffusion coefficient of the nonspecifically bound protein along the DNA, L is the total length of the DNA molecule, l_d is the maximum DNA contour distance $x_{max} - x_{min}$ covered by the protein before dissociation, c is the concentration of the target, and $\left(\frac{l_{seq}}{l_d} + \frac{D_3}{D_1} l_{seq} L l_d c \right)^{-1}$ is the acceleration factor

to $k_{a,3D} = D_3 l_{seq}$. In order to evaluate the facilitated diffusion model directly, it is necessary to know D_1 and l_d , which can only be obtained by imaging protein-DNA binding dynamics using single-molecule measurements. In fact, if these values do not fall within a certain range, “facilitated” diffusion can actually slow the search times.

Note that in this facilitated-targeting rate calculation (and other numerous calculations), sliding was assumed to be the DNA sequence-insensitive Brownian diffusion for all timescales [15, 21, 29, 30]. In the Brownian sliding model, the 1D mean square displacement of proteins on DNA is $\langle \Delta x^2 \rangle = 2D_1 t$, where D_1 is the 1D sliding diffusion coefficient and t is the observation time. Should protein translocation follow a different model from Brownian motion (i.e., if D_1 is time dependent as $D_1(t)$, or if the time dependence $\langle \Delta x^2 \rangle$ of differ from the power of one), the protein search speed through DNA sequences will change. As a consequence, the effect of facilitated diffusion on the protein’s target association rate will vary.

2.2.2 Experiments

We used a LacI fusion-protein consisting of a green fluorescent protein (GFP)–GFP13 (S65T):*lacI-I12* fusion (GFP-LacI), and stained the DNA with the dimeric cyanine dye BOBO-3. DNA constructs of Lambda Zap vector with 256 tandem copies of *lacO* (*lacO*₂₅₆) were used. *LacO*₂₅₆-DNA was 42.06 kbp long with a contour length of 14.3 μm , and the 9.22 kbp *lacO*₂₅₆ insertion started at 24.02 kbp. The nonspecific sequences of the DNA construct are identical to that of λ DNA. The synthesis methods for the fusion protein and the *lacO*₂₅₆-DNA, and the sample preparation method are described in [31]. There were *lacO*₂₅₆-DNA dimers as well as monomers in the solution; the dimers were formed by the sticky-end-hybridization of two *lacO*₂₅₆-DNA monomers (Fig. 2.2a). After the LacI-DNA and BOBO-3 incubation, the GFP-LacI concentration was 50 nM and the *lacO*₂₅₆-DNA concentration was 11 pM (0.3 $\mu\text{g}/\text{ml}$). The DNA intercalating cyanine dyes are known to stretch DNA by 30% in length at 1 dye/5 bp [32], so at our concentration of 1 dye/10 bp, the DNA molecules were stretched by 15% to 16 μm . Since BOBO-3 produced no obvious effect on the DNA-configuration-dependent LacI-DNA

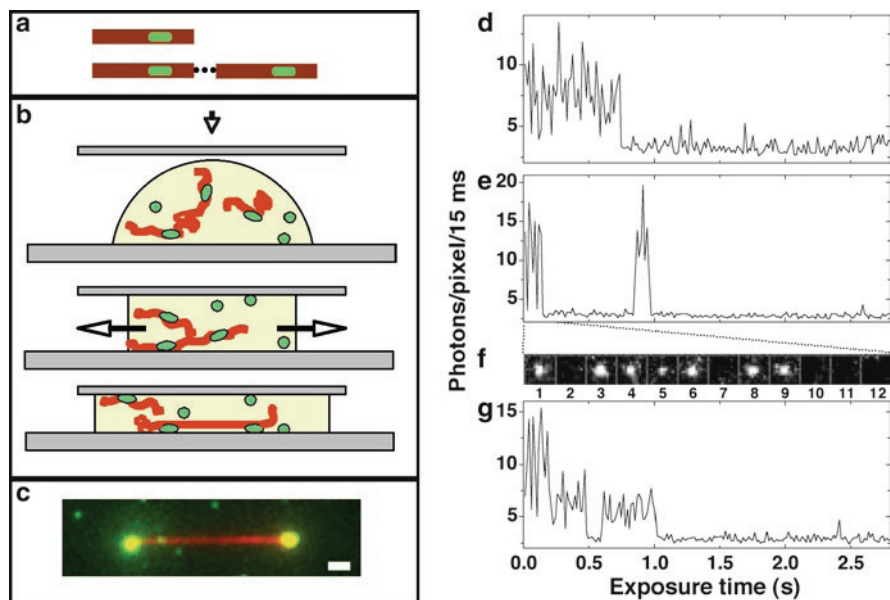


Fig. 2.2 (a) Schematics of a GFP-LacI (green) bound *lacO*₂₅₆-DNA monomer and dimer (red). (b) Elongation of the DNA. (c) Frame-averaged superposed image of GFP-LacI bound to an elongated *lacO*₂₅₆-DNA dimer. The scale bar is 1 μm . (d) A GFP-LacI monomer of frequent blinking and unitary bleaching. (e) A GFP-LacI monomer that blinked, recovered the first bleaching in 3 s, and finally irreversibly bleached. (f) The GFP-LacI dots for the first 12 frames of (e), showing blinking at frames 2 and 7, and bleaching at frame 10. (g) A GFP-LacI dimer with two bleaching events

specific binding [31], we expect that its effect on the LacI DNA-specific binding (which is less DNA-configuration dependent) will be negligible [33]. A catalytic oxygen scavenging solution was used to maximize dye lifetimes [31]. 1 μ l of the DNA+LacI solution and 4 μ l of the oxygen scavenging solution were deposited onto a fused-silica chip.

A glass cover slip was used to flatten the solvent, and the edges of the cover slip were then sealed with nail polish. As the cover slip flattened the droplet, hydrodynamic flow elongated the DNA dimers, and the two LacI-*lacO*₂₅₆ sites stuck to the surface, creating an anchored elongated DNA molecule (Figs. 2.2b, c, and 2.3c) stretched up to 90% of its native contour length. The tension on DNA was a few pico-Newtons [34]. DNA was not observed to stick to fused-silica surfaces at our pH of 8.0 and BSA concentrations, and the elongated DNA molecules were effectively suspended from the surface, as evidenced by the DNA's transverse motion of ± 50 nm (data not shown). Thus, unbound GFP-LacI molecules interacted only with free unattached and nonspecific DNA. Note that the sticking of GFP-LacI to fused-silica surfaces occurred only at the deposition step as the air–water interface moved over the chip surface. After the cover slip was sealed, the free GFP-LacI molecules (≈ 2 nM) diffused in the solution freely and did not stick to the surface, as evidenced by observation of the freely diffusing GFP-LacI near the surface (data not shown).

The single-molecule experiments were performed using a prism-type Total Internal Reflection Fluorescence Microscopy (TIRFM) method (Fig. 2.3a and b). The laser excitation was synchronized to the 3.4 Hz data acquisition rate of the I-CCD camera. The emitted photons from BOBO-3 and GFP were collected using a 100X TIRF oil-immersion objective (N.A. = 1.45), went through a custom-designed dichroic mirror and emission filter set (Chroma Technology

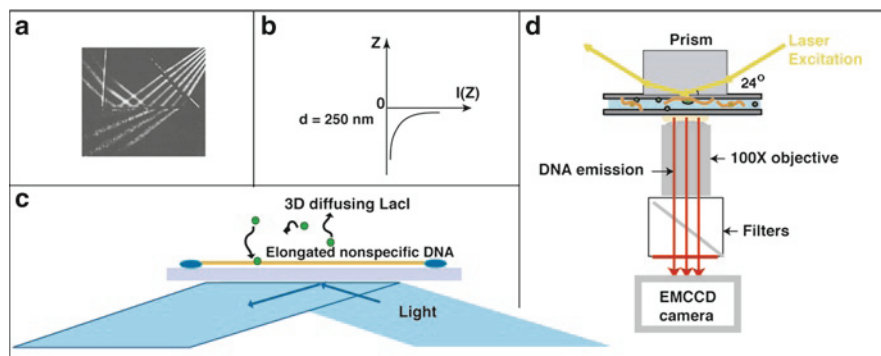


Fig. 2.3 Schematics of our experimental setup. (a) Light goes from air into a prism. At the prism–water interface, TIRF occurs at an inclination above the critical angle. (b) The decay of the evanescent light intensity $I(z)$ in z direction. The penetration depth d is ≈ 250 nm. (c) Schematic of our protein–DNA interaction system. A single DNA molecule (orange) is elongated along the fused-silica surface (grey) for TIRF imaging (blue light), and the 3D diffusing LacI molecules (green) run into the DNA molecule and bind to it. (d) Schematics of our imaging system. DNA and proteins are excited by yellow and blue laser light, respectively, and the emission photons go through an 100X objective and are collected by a single-photon sensitive CCD camera

Corp, Rockingham, VT), and were recorded by an I-CCD camera (I-PentaMAX:HQ Gen III, Princeton Instruments, Trenton, NJ; Fig. 2.3d). The PSF width of the diffraction-limited optical system was measured to be 280 nm, and the imaging pixel size was 117 nm. The pixel count of the camera was converted to a photon count using known conversion factors [31]. The mean 488 nm illumination intensity over the illumination areas of $30\ \mu\text{m} \times 50\ \mu\text{m}$ was $1000\ \text{W}/\text{cm}^2$. The centroid location of a GFP-LacI dot was determined by fitting its 1D fluorescence intensity profile to a Gaussian. The number of detected photons per PSF per frame (between 50 and 300 photons) limited the position measurement accuracy to be between 10 and 50 nm [35].

Knowledge of the fluorescence characteristics of single free GFP-LacI monomers and dimers attached to fused-silica surfaces is essential in determining the single-molecule nature of a bound protein. GFP-LacI monomers blink frequently (short fluorescence dips to near instrumental noise level), and bleach with no recovery (Fig. 2.2d). At our excitation intensity of $1000\ \text{W}/\text{cm}^2$, mean exposure time of 10 ms, and synchronized imaging frequency of 3.4 Hz, the mean net observation time of each GFP-LacI molecule was 5 s before it bleached (giving a total laser exposure time of 0.15 s). The mean number of photons emitted by the bound GFP-LacI molecules before bleaching was $\approx 4 \times 10^4$ photons. This 5 s observation time gave the *instrumental* limit to the maximum mean distance we observed GFP-LacI motion on DNA in this experiment.

2.2.3 Results and Analysis

An image sequence of a single GFP-LacI molecule diffusing along DNA is shown in Fig. 2.4b. This is 1 out of 70 walks that were observed and chosen for its large net displacement. Figure 2.4a shows the frame-averaged superposed image of the anchored DNA and the diffusing GFP-LacI on DNA. Time-lapse images of the diffusing protein show clear relative displacements (Fig. 2.4b), with one immobile anchoring site used as a reference point. We know that we were observing a single GFP-LacI dimer from the fluorescence time trace in Fig. 2.4d, which clearly shows two bleaching steps. Both GFP-LacI monomers (80%) and dimers (20%) have been observed to diffuse on DNA. As is evident in Fig. 2.4d, fluorescence time traces of bound GFP-LacI molecules were identical to that of single immobile GFP-LacI (Fig. 2.2d-g), with the same blinking rate and characteristic bleaching time of $\approx 0.15\ \text{s}$ (5 s net observation time). The DNA locations of the diffusing protein at different frames are correlated and localized, thus at $D_3 = 10^8\ \text{nm}^2/\text{s}$ and our protein concentration of a few proteins/ μm^3 , the chance for two different proteins landing consecutively on the same location of DNA is 1 in 1000. Figure 2.4d plots the distribution of all relative displacements $\langle D_1 \rangle =$ of the walk. This is a Gaussian of SD = 130 nm centered near zero, which is typical for Brownian motion with limited data points.

Now, we discuss our analysis showing that individual protein diffusion trajectories, which consist of multiple measurements x_i until the protein disassociates, are

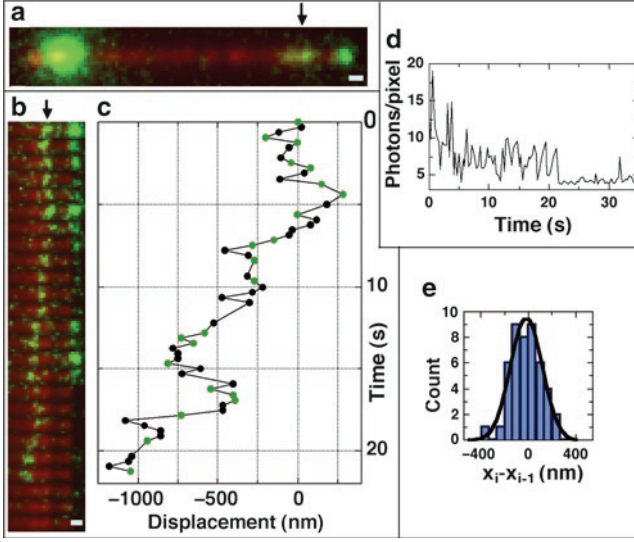


Fig. 2.4 (a) Frame-averaged, superposed image of a GFP-LacI molecule diffusing along DNA. The two *large dots* at the DNA ends are LacI-lacO₂₅₆ sites, and the *green segment* on the nonspecific DNA (*arrow*) is the trace of the diffusing GFP-LacI. (b) Image series of the diffusing protein (*arrow*) of selected clear relative displacements corresponding to *green dots* in (c), the displacement versus t curve of the diffusing protein. (d) Fluorescence time trace of the diffusing GFP-LacI. It is a dimer. (e) Gaussian distribution of $x_i - x_{i-1}$. The scale bar is $0.5 \mu\text{m}$

Brownian in nature, and we obtain 1D diffusion constant D_1 for these trajectories. Qian et al. have derived an expression to tell (1) whether a single diffusion trajectory is Brownian and if so (2) obtain the diffusion constant of the trajectory [36]. This method calculates the mean square displacement $\text{MSD}_{(n, N)}$ for all available time intervals of a single diffusion trajectory

$$\text{MSD}_{(n, N)} = \frac{\sum_{i=1}^{N-n} (x_{i+n} - x_i)^2}{N - n} = 2D_1 n \Delta t + 2\sigma_s^2, \quad (2.2)$$

where, N is the total number of positions measured, n is the measurements index going from 1 to N , Δt is the time interval between two consecutive position measurements, and σ_s is the measurement accuracy associated with each x_i . We can obtain D_1 of a single diffusion trajectory from its $\text{MSD}_{(n, N)}$ to high precision by weighted linear-fitting $\text{MSD}_{(n, N)}$ to n , taking $\text{MSD}_{(n, N)}$'s variances at different n into consideration. As n increases, the number of available measurement points for $\text{MSD}_{(n, N)}$ averaging decreases, and the variance in $\text{MSD}_{(n, N)}$ increases as

$$\sigma_{n, N}^2 = (2D_1 n \Delta t)^2 (2n^2 + 1) / [3n(N - n + 1)]. \quad (2.3)$$

If a single trajectory is Brownian, then its $\text{MSD}_{(n, N)}$ at n below a cutoff n_c will be a linear function of t , with n_c determined by a set fractional $\text{MSD}_{(n, N)}$ uncertainty in Eq. 2.3. We chose n_c to be where $\sigma_{n, N} / (2D_1 n \Delta t)$ is 50%. We plot $\text{MSD}_{(n, N)}$ versus n

for trajectories with $N > 10$, where there are at least three $\text{MSD}_{(n,N)}$ values whose fractional variances are $< 50\%$ Eq. 2.3. We also used only trajectories with less than five contiguous GFP blinks. Since $\sigma_s < 50$ nm, $\text{MSD}_{(n,N)}$, which is the square of the difference of two position measurements, has an offset of $2500 \text{ nm}^2 < 2\sigma_s^2 < 5000 \text{ nm}^2$. These photon noise offsets were subtracted in the $\text{MSD}_{(n,N)}$ versus n curves.

Figure 2.5a plots displacement x versus time for 70 trajectories. The 15 trajectories in color are the walks for which we have obtained D_1 , and the center black line is a stationary GFP-LacI stuck to the fused-silica surface (not DNA). Figure 2.5c plots $\text{MSD}_{(n,N)}$ versus n for these 15 trajectories in linear scale and Fig. 2.5d in log-log scale at low n values, respectively. The log-log plots are all straight lines with the slope of 1 at low n , clearly indicating that the 1D trajectories are Brownian motions. The dashed line in Fig. 2.5d is a fit of 2 with weighted error 3 to all n points below n_c of the topmost trajectory. The intercepts at $n = 1$ are $2D_1\Delta t$ for each particular walk, as can be seen by inspection of 2 (Fig. 2.5d). Thus, while all the walks are Brownian in nature, the different intercepts at $n = 1$ indicate that there is a large distribution in diffusion coefficients and there is not a unique, single value for D_1 . We also plotted the distributions of nondegenerate relative displacements $x_i - x_{i-n}$ for the first 15 positions of all 70 trajectories for $n = 1, 2$, and 3 in Fig. 2.5b; the displacements are all Gaussians centered at zero with SD increasing with n . This result further demonstrates that LacI's diffusion trajectories are truly Brownian in nature, regardless of the variations in individual diffusion coefficients. Two other papers on single-molecule imaging studies of

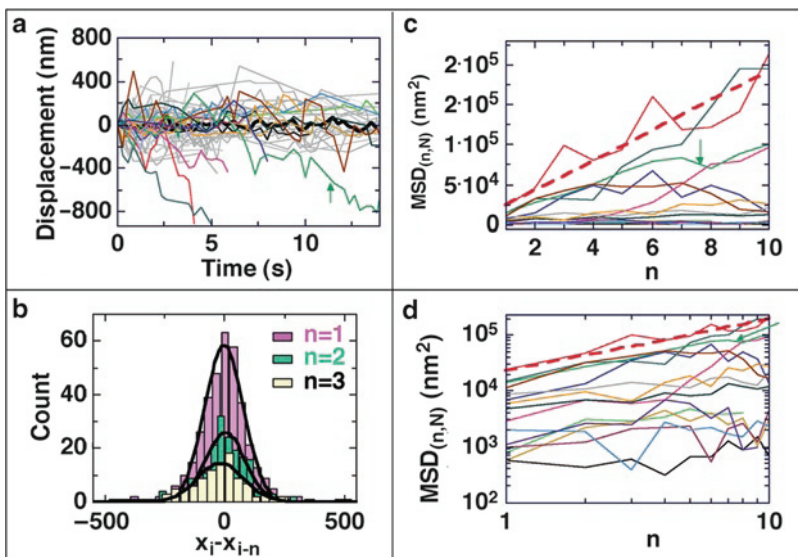


Fig. 2.5 (a) x versus t for 70 trajectories. (b) Nondegenerate $x_i - x_{i-n}$ distributions. (c) $\text{MSD}_{(n,N)}$ versus n for the 15 colored walks in linear scale and (d) in log-log scale. The arrows in (a), (c), and (d) denote the walk in Fig. 4. The dashed lines in (c) and (d) are the fit of 2 to the top trajectory

protein diffusion on DNA were published in the same year (2006) [37, 38], with [38] reporting a similar large distribution in 1D diffusion coefficients for Rad51 on aligned DNA molecules, so our result here may be of some generality.

Figure 2.6a shows the distribution of the 15 D_1 values (corrected to DNA contour length), which span a large range from $2.3 \times 10^2 \text{ nm}^2/\text{s}$ to $1.3 \times 10^5 \text{ nm}^2/\text{s}$. Figure 2.6b shows that the different D_1 values are distributed randomly along the DNA, showing a lack of correlation between the D_1 and the regions on the λ DNA on which the protein has diffused. Figure 2.6c shows the distribution of the l_d in DNA contour length. Because λ DNA has large sequence variance in the nonspecific region with $\pm 30\%$ difference in local AT and CG concentrations, it is possible that the diffusion constants are a function of local sequence. It is also possible that the large distribution in D_1 is caused by conformational distributions in the protein [39]. Further experiments are needed to answer these questions.

Finally, we use our data to examine the question of the extent to which facilitated diffusion can enhance the LacI target binding rate. Just as there is a distribution in the 1D diffusion coefficient D_1 , there is also a distribution in the diffusion lengths l_d , whose value is further compromised by the mean observation time to bleaching of the GFP of 5 s. Since the final target binding is the result of many diffusion events

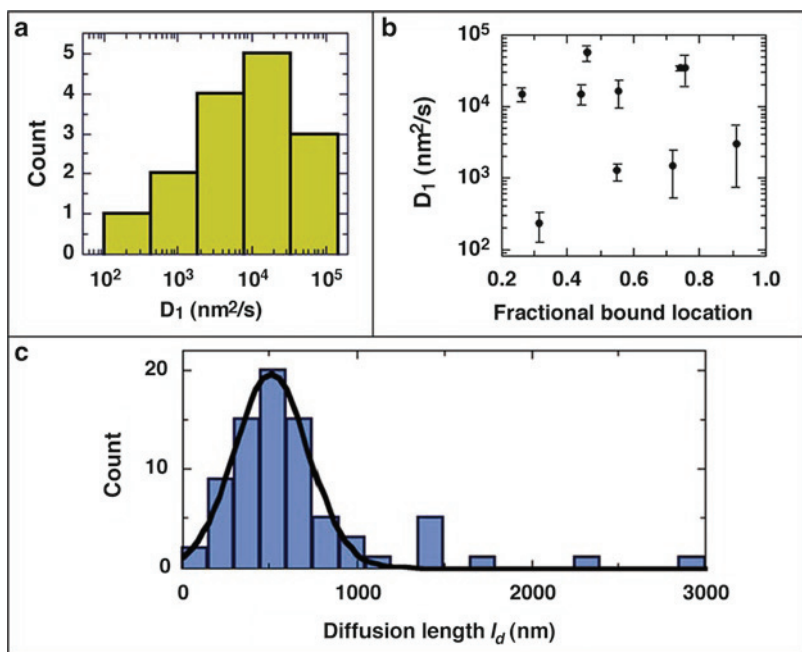


Fig. 2.6 (a) D_1 distribution of the 15 trajectories. (b) D_1 versus fractional bound location on the nonspecific segment of the LacO_{256} -DNA dimer. The error bars were obtained from the fit of $\text{MSD}_{(n,N)}$ to n with weighted errors at each n given by 3. (c) Histogram of $x_{\max} - x_{\min} = l_d$ for the 70 trajectories. The solid line is a Gaussian fit with a mean of $500 \pm 220 \text{ nm}$ (mean \pm SD). Values in (a) and (c) have been adjusted to DNA contour length

on nonspecific DNA, we use the mean $\langle l_d \rangle$ (probably a lower bound due to bleaching) of 500 nm, and the mean diffusion coefficient of $\langle D_1 \rangle = 2.1 \times 10^{-10} \text{ cm}^2/\text{s}$ in 1. Also using Riggs' concentration of 1 *lacO*/1670 μm^3 , $D_3 \approx 4 \times 10^{-7} \text{ cm}^2/\text{s}$ for LacI tetramers ($a \approx 10 \text{ nm}$), and $L = 15.5 \mu\text{m}$, the accelerating factor in 1 is 93 ± 20 , which thus resolves the 100-fold discrepancy between the theory and the experimental data. We conclude from these measurements that facilitated diffusion increases the LacI-*lacO* binding rate well over the apparent diffusion limit. This result demonstrates that facilitated diffusion in the form of 1D Brownian motion is the mechanism responsible for the faster-than-diffusion binding of LacI to *lacO*, and quite possibly, the reason also for the observed faster-than-diffusion binding in other protein-DNA interactions.

2.2.4 Concern for the Interpretation of the “Sliding Length” $\langle l_d \rangle$ and D_1

There are two concerns for the above interpretation of experimental results: (1) The observed mean “sliding length” $\langle l_d \rangle$, which is the maximum DNA contour distance $x_{\max} - x_{\min}$ covered by the protein before dissociation, quite likely is not the pure sliding length defined in Eq. 2.1; rather it is the combined distance of many sliding and hopping cycles before the permanent dissociation of proteins from DNA. This statement stems from the estimation that LacI's nonspecific DNA dissociation rate constant is on the order of milliseconds ($\approx 0.6 \text{ ms}$ to 5 ms , or milliseconds to seconds) [3, 19, 21, 30]. (2) For the same reason, D_1 is the “effective” 1D diffusion coefficient of the combined sliding and hopping trajectory in the time-scale of seconds, rather than the pure sliding diffusion coefficient.

With the three questionable parameters in Eq. 2.1 – (1) Brownian sliding (Sect. 2.2.1), (2) the sliding length (Sect. 2.2.3), and (3) the 1D diffusion coefficient D_1 (Sect. 2.2.3) – the LacI target association rate calculation due to facilitated diffusion should be reevaluated. In order to correctly calculate facilitated target association rate using Eq. 2.1, the true sliding displacement versus time relation, sliding length, and sliding dissociation rate constant should be obtained.

2.3 New Challenge: Millisecond Timescale Single-Molecular Tracking

To reiterate key limitations of the above LacI diffusion experiments in the time-scale of seconds for sliding mechanism studies of LacI on DNA: (1) We know that the LacI proteins stay around DNA for the observation time of seconds; what we do not know is whether the proteins slide for the whole time or many hopping cycles are convolved. (2) If the protein diffusion pathway on DNA is a combination of sliding and hopping, the sliding-hopping-alternation kinetics is not known

(i.e., the mean sliding time t_d and hopping time t_{hop} are not known). (3) In the sliding motion, how the protein displacement changes with time is not known. These three factors must be addressed for correct calculation of the target association rate of proteins.

Faster single-molecule tracking than the current centroid tracking method in seconds timescales appears to be the answer to the above three questions. Then, how much faster is fast enough? For (1) and (2), millisecond tracking resolution may be sufficient according to Sect. 2.2.4. For (3), the sliding motion characteristics studies, is milliseconds tracking also sufficient? Below, we list predicted displacement versus time characteristics of different sliding models in 10^{-7} s to 1 s timescales.

Other than the DNA-sequence-independent Brownian sliding model, the alternative sliding models are the DNA-sequence-dependent sliding models. There are four simple DNA-sequence-dependent models describing four different protein translocation energy landscapes along a stretch of DNA sequences (Fig. 2.7a I–IV): (1) The energy at each binding site n is independent of others. The translocation energy barrier from site n to site $n' = n \pm 1$ is the difference between the protein binding energies of the two sites, if positive and zero, if negative [22, 40]. (2) In order to move from site n to site n' , the protein needs to completely dissociate from the DNA first over a threshold level $EM = \text{Max}[E(n)]$. The translocation energy barrier is $EM - E(n)$ [22]. (3) The threshold energy Et is lower than EM , and the translocation energy barrier is the maximum of the energy differences and zero – $\text{Max}[Et - E(n), E(n') - E(n), 0]$ [22, 41, 42]. (4) Two-state model in which Et separates the reading regime ($E(n) < Et$), where the translocation is the same as in model III from a sliding regime ($E(n) > Et$), where the sliding motion is on a flat energy landscape [22, 43, 44].

In contrast to the DNA-sequence-independent sliding model, where the translocation mechanism yields Brownian diffusion for all timescales as $\langle n^2 \rangle = 2D_t t$ the four DNA-sequence-dependent protein translocation mechanisms predict distinct diffusion patterns at different timescales. Figure 2.7b shows the mean square displacement versus time ($\langle n^2 \rangle$ versus t) log–log plots of the four sequence-dependent diffusion models from $t = 5 \times 10^{-7}$ s to 1 s. All diffusions are Brownian with the $\langle n^2 \rangle$ versus t slope of one in the log–log plot at $\approx t > 30$ ms (left vertical dashed line). At $t < 30$ ms, all models exhibit subdiffusion behavior, in which $\langle n^2 \rangle$ is proportional to $A(t)t^{b(t)}$, with $b < 1$ ($b[t]$ being the slope of the lines at time t and $\log(A[t])$ being the vertical offset of the line, according to the expression $\log\langle n^2 \rangle = \log A[t] + b[t] \log t$).

It is clear that diffusion studies of sliding below 30 ms are necessary to differentiate Brownian sliding from subdiffusive sliding, provided that sliding lasts longer than 30 ms. This 30-ms tracking resolution cannot be afforded by the current centroid method, which is limited to temporal resolution of 300 ms (see Sect. 2.4.1), let alone 1 ms sliding time. While the diffusion of proteins on DNA in the timescales of seconds has been reported in many recent single-molecule protein–DNA interaction studies [20, 37, 38, 45–48, 48–56], no millisecond timescales studies have been reported. Alternative higher temporal resolution single-molecule

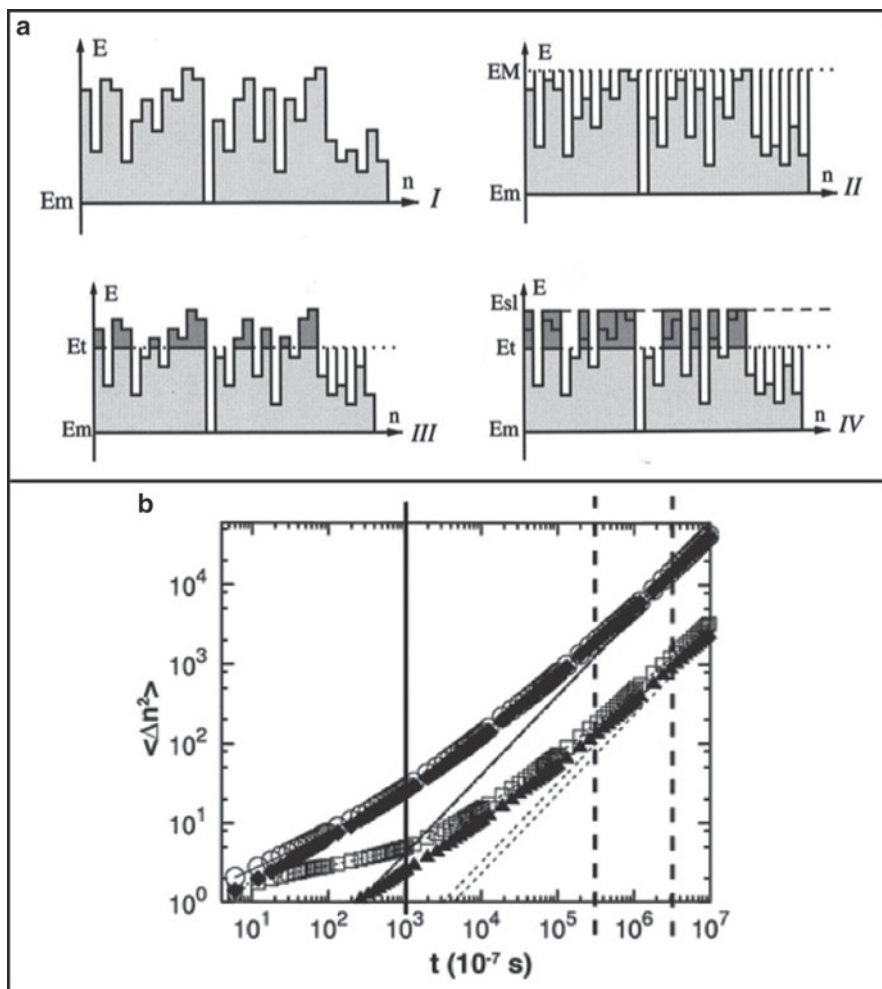


Fig. 2.7 Protein translocation models and the corresponding diffusions, adapted from [22]. In the calculations of total bound energy between a protein and DNA bases, the hydrogen bond energy between each base pair and the protein used is ε . (a) Schematics of the four energy landscapes for translocation of RNA-polymerase along 30 base pairs T7 DNA. E_m is the minimum protein interaction energy and E_t is the maximum interaction energy of all base pairs. The threshold level E_t (dotted line) is set to E_m for model II and to an intermediate value for models III and IV. For model IV, all energy levels above E_t are redefined to a common sliding energy E_{sl} (dashed line). (b) Mean square site displacement $\langle \Delta n^2 \rangle$ versus t for the four different models, with $\varepsilon = k_B T$ and $E_t = 0$. Model I, circles; model II, triangles; model III, diamonds; model IV, squares. The slanted straight lines with slope of one, indicating the slope of Brownian motions, are fits to the models from 0.6 to 1 s. The solid vertical line marks 0.1 ms, the lowest timescale for our studies using single-molecule image deconvolution. The left vertical dashed line at 30 ms, where the subdiffusive curves begin to deviate from the Brownian diffusion line, marks the fastest camera frame rate for centroid measurements in the high camera-reading-noise regime (without pixel binning and partial screen imaging). The right vertical dashed line at 300 ms marks the fastest camera frame rate in the low camera-reading-noise regime

millisecond timescale studies are necessary. Below, we describe our new single-molecule image deconvolution method to study the subexposure dynamics of single mobile fluorescent molecules with millisecond temporal resolution and nanometer spatial resolution. In Sect. 2.4, we use this method to analyze images of diffusing LacI on DNA with exposure times approaching the predicted nonspecific DNA dissociation time $t_d \approx 1$ ms.

2.4 Pushing the Envelop: Single-Molecule Imaging with Higher Temporal and Spatial Resolution

In this section, we introduce single-molecule image deconvolution (SMID) as a new method with increased temporal and spatial resolution for single-molecule tracking measurements.

2.4.1 *Rationale for Developing the Single-Molecule Image Deconvolution Method*

Ideally, to discern subdiffusive sliding models from the standard Brownian sliding model, centroid versus time measurements should be used to obtain $\langle n^2 \rangle$ versus t relation at all timescales down to below $t_d \approx 1$ ms. However, current single-molecule imaging EMCCD cameras (Photomax, Andor, etc.) do not offer faster than 10 MHz pixel reading speed, which in the high background noise regime corresponds to a 30-Hz frame reading rate (or 100 Hz with pixel binning and partial screen imaging, although binning is not recommended due to loss of PSF information) and in the low background noise regime to 3 Hz (or 10 Hz). These maximum frame rates correspond to temporal resolutions of centroid measurements between ≈ 30 and 300 ms. Does this mean that one can study 30 ms diffusion characteristics with centroid measurements? The answer is no. Tracking more than 10 centroids of the molecule at different times is necessary for studying single-particle diffusion characteristics [36, 45], and this requirement lifts the centroid measurement temporal resolution to 0.3 s in the high camera-reading-noise regime (right vertical dashed line in Fig. 2.7b) and to seconds in the low camera-reading-noise regime.

Thus, in order to discriminate different displacement versus time characteristics at millisecond timescales, centroid measurements with the best temporal resolution of 100 ms (high background noise regime and loss of spatial resolution due to pixel binning; not suggested for single-molecule tracking studies) are not sufficient. The single-molecule image deconvolution method introduced below will have millisecond temporal resolution and nanometer spatial resolution for single-molecule tracking.

2.4.2 Single-Molecule Image Deconvolution (SMID)

A Gaussian fit to the PSF of a single fluorophore contains two fitting parameters: centroid and standard deviation (SD, denoted by s in this chapter). The centroid is considered the center of the PSF, while the SD is the width of the PSF (Fig. 2.8d). In contrast to centroid measurements, which have been extensively used for 1D and 2D localization studies, PSF SD measurements have played little role in single-molecule tracking studies. However, the SD of a point light source can carry additional localization and dynamic information about the particle that is inaccessible by centroid measurements: (1) for a stationary molecule, the axial location (distance away from the focal plane) of the particle can be obtained only from SD measurements [57–59] and (2) for a moving particle, regardless of exposure time, the captured image will contain additional blurring. Figure 2.8 shows that the moving molecules in (b) and (c) are obviously blurred compared to the stationary molecule in (a). In one recent study, SD measurements of a moving GFP-LacI in *E. coli* have been reported [37]; however, for both immobile and mobile single molecules, correct interpretation of the SD values requires further theoretical and experimental studies. Here, we introduce an algorithm to deconvolve the blurred image of a moving molecule to obtain its trajectory during exposure by measuring the SD of the image.

Our single-molecule image deconvolution method uses a mathematical algorithm that deconvolves the blurred snapshots of a moving molecule with subexposure

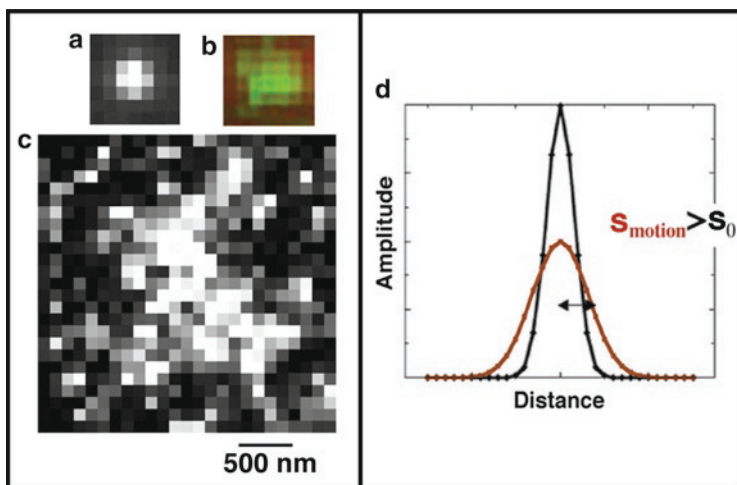


Fig. 2.8 (a) An immobile GFP-LacI molecule on surface, (b) an 1D diffusing GFP-LacI molecule on DNA, (c) a 3D diffusing GFP-LacI molecule in solution. The SDs of the PSF are larger for the diffusing LacI molecules. (d) Schematic Gaussian PSF of immobile (black) and diffusing proteins (red); SD of the diffusing protein s_{motion} is $>$ than that of the immobile one s_0

temporal resolution. This method is based on the principle that a fluorescent particle emits photons along its pathway throughout the whole exposure time, and the number of photons emitted at a specific position x depends on the net time the molecule spends at that position during the exposure. We introduce the pathway distribution function $g(x)$ to describe the net time distribution that a single fluorescent molecule spends at location x during the exposure. The final fluorescence intensity profile $I(x)$ of the moving molecule is the convolution of the molecule's PSF $f(x) \propto \exp(-x^2 / 2s_0^2)$ and its pathway distribution function $g(x)$,

$$I(x) \propto f(x) * g(x), \quad (2.4)$$

where s_0 is the SD of the PSF of the immobile molecule at focus. By fitting the final convolved snapshots of a moving single molecule to Eq. 2.4, we can extract the appropriate $g(x)$. We call this procedure for obtaining the pathway distribution $g(x)$ for a convolved image of a moving single fluorophore the *Single-Molecule Image Deconvolution (SMID) method* [60].

There could be more than one suitable pathway that yields the same convolved image. It is fortunate, however, that there are usually only a few theoretical models from which to choose. By combining SD measurements with the additional centroid-versus-time information at different timescales in the analysis, the $g(x)$ selection can be narrowed to fewer possibilities.

2.4.3 Precision Analysis Associated with SD Measurements

In order to use SMID to discern different subexposure time pathways, which in our case reflect different sliding mechanisms and sliding-hopping-alternation kinetics, it is important to obtain the precision of SD measurements. If the expected SD values of various models differ by more than the error of the experimentally measured SD for each model, the models can be differentiated. We have performed the full SD measurement error analysis for single immobile fluorescent molecules at focus [61].

Error analysis for centroid measurements of immobile molecules has been thoroughly investigated and applied to many systems [35, 62]. As with the centroid measurements, the precision of SD measurements is affected by the same experimental settings of a finite number of photons per PSF N , the camera background noise standard deviation σ_b , and the camera's finite pixel size a . We have derived an analytical expression for PSF SD measurement error as a function of these parameters. The SD measurement error in x or y direction is the square root of the mean square error $\langle(\Delta s_i)^2\rangle$

$$\langle(\Delta s_i)^2\rangle = \frac{s_0^2 + \frac{a^2}{12}}{N} + \frac{16\pi \left(s_{0x}^2 + \frac{a^2}{12}\right)^{3/2} \left(s_{0y}^2 + \frac{a^2}{12}\right)^{1/2} (\sigma_b^2 + \langle b \rangle)}{3a^2 N^2}, \quad (2.5)$$

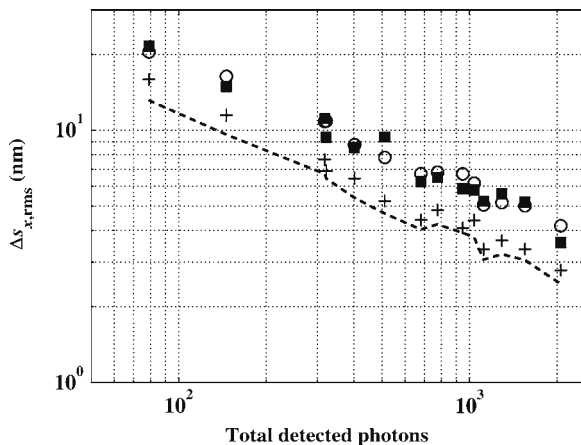


Fig. 2.9 SD measurement error, $\Delta s_{x,rms}$, versus the number of detected photons N studied by using four different methods: experimental measurements (*solid squares*), simulations (*circles*), numerical integrations (*crosses*), and analytical calculations (*dashed line*). Each experimental $\Delta s_{x,rms}$ data point is the SD of a Gaussian fit to the s_x distribution of a single streptavidin-Cy3 monomer adsorbed to surfaces

where, $\langle b \rangle$ is the mean background photon count. Figure 2.9 shows our SD measurement error results using four methods of study: experimental measurements, simulations, numerical integrations, and analytical calculations. At low PSF photon count of $N \approx 100$, the SD error is ≈ 15 nm; at high PSF photon count of $N \approx 1,000$, the SD error is ≈ 4 nm. This SD error expression is approximately 1.25 times higher than the precision of centroid measurements under comparable experimental conditions. The experimental results in Fig. 2.9 were obtained using a different camera (Andor EMCCD), a different excitation wavelength of 532 nm, and a different pixel size of $a = 79$ nm from the measurements in Sect. 2.2. In addition, 2D Gaussian fitting to PSF was used instead of the 1D fitting in Sect. 2.2.

2.4.4 SMID Enables Single-Image Molecular Dynamics Studies

In the above section, we introduce a new method, SMID, for single-molecule localization and tracking studies with higher temporal and spatial resolution than currently afforded by centroid measurements. The higher temporal resolution is achieved through the following mechanism: while many centroid measurements at different times are required for tracking a single molecule, SD measurement of only one image can offer insight into single-molecule dynamics at the shorter subexposure timescales with higher precision. Literally, one millisecond exposure image can be used to differentiate mechanisms that differ in SD by nanometers, enabling single-image studies

of molecular dynamics with at least 100-fold improvement in temporal resolution. For the spatial resolution, while centroid analysis is based on measuring the mean location of the molecule for each image during the exposure time, measurement of the PSF SD provides a quantitative description of the molecule's spatial distribution. Consequently, the additional information extracted from this distribution constitutes improvement in spatial resolution. These improved temporal and spatial resolutions enable description of SMID studies with another term – single-image molecular analysis (SIMA) studies [60].

Our analytical expression of the PSF SD error provides the level of precision for SMID measurements of single immobile fluorescent molecules. When this expression is extended to axial localization and subexposure time studies, the dynamics of various very similar biological systems investigated *in vitro* and *in vivo* can be elucidated and their underlying mechanisms differentiated, such as our studies on differentiating sliding mechanisms of proteins on DNA. When the difference between the SDs measured for molecules displaying different characteristic motions is small, our error analysis will serve as a means for proper discrimination. SMID with full error analysis should be applied to reanalyze existing single-molecule tracking studies, as well as to all future fluorescence particle tracking experiments for a more thorough description of a particle's dynamics.

2.5 Application of SMID to LacI Diffusion on DNA Studies

Now, we discuss preliminary results and considerations about the application of SMID to LacI diffusion on DNA studies. Issues relevant to the interpretation of experimental results for the correct diffusion model selection are discussed.

2.5.1 SD Measurements of Diffusing LacI on DNA

Figure 2.10 shows 1D SD measurements for diffusing GFP-LacI on DNA using exposure times of 5, 10, and 15 ms (using the same set of data in Sect. 2.2). To illustrate that the SDs of moving proteins differ from that of stationary proteins, s_x distributions of diffusing proteins are compared to s_0 distribution of stationary proteins. The mean of the s_0 distribution, $\langle s_0 \rangle = 132 \text{ nm}$ indicates that our imaging system is diffraction limited (Fig. 2.10a), and the SD of the s_0 distribution is the error associated with each PSF SD measurement using our imaging system. In Fig. 2.10b, the mean and spread of the diffusing proteins' s_x distribution at 5 ms exposure are $165 \pm 32 \text{ nm}$ (mean \pm SD), and they are apparently larger than those of the stationary proteins of $132 \pm 23 \text{ nm}$. Figure 2.10c shows that as exposure times increase to 10 ms and 15 ms, $\langle s_x \rangle$ values increase accordingly, to $176 \pm 50 \text{ nm}$ and $183 \pm 62 \text{ nm}$, respectively.

Although Fig. 2.10 validates the applicability of SMID for protein diffusion on DNA studies, the data may not be directly useful for sliding dynamics analysis. For

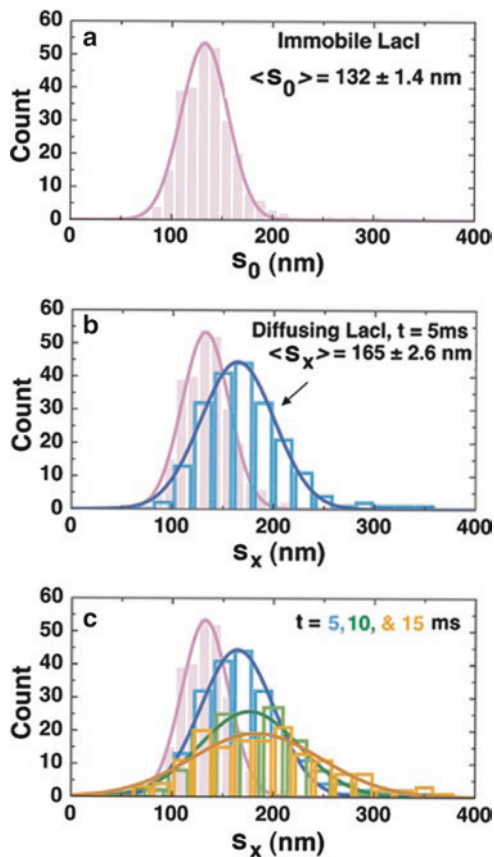


Fig. 2.10 (a) s_0 distribution of immobile GFP-LacI (pink) with $\langle s_{0,x} \rangle = 132 \pm 1.4$ nm (mean \pm error to the mean). (b) s_x for diffusing GFP-LacI on DNA at 5 ms exposure time (blue) with $\langle s_x \rangle = 165 \pm 2.6$ nm. (c) s_x distributions for 5, 10, and 15 ms exposure times, and the $\langle s_x \rangle$ values are 165 ± 3.5 nm, 176 ± 4.5 nm, and 183 ± 5.2 nm, respectively

exposure times of 5–15 ms, whether hopping motion is convolved in the images, and if so, the extent to which it is convolved are unknown. These unknowns render the data insufficient for studying the sliding movements of proteins without a full analysis of their hopping motions as well.

2.5.2 Exposure Times of 0.1–2 ms Should Be Used for LacI Sliding Studies

For LacI sliding studies, shorter exposure times of 0.1–2 ms should be used. We chose this range of exposure times for three reasons: (1) 0.1 ms is the shortest exposure time at our peak laser power to detect PSF with a signal-to-noise ratio of more than 3;

(2) 0.1–2 ms falls within the range of the current estimated dissociation time of LacI from nonspecific DNA. In references [19, 21], the dissociation time of LacI from non-specific DNA was calculated using experimental results to be between 0.3 and 5 ms in vivo in *E. coli*; alternatively, when the theoretical limit of association was used for calculation, the dissociation time is between 1 ms and 1 s [3, 30]. Although there have not been experimental measurements of the LacI's nonspecific DNA dissociation rate constant, our exposure times should satisfy a majority of the estimated dissociation times to guarantee that we will be imaging the sliding motion with minimal perturbation from hopping; and (3) the expected SDs for Brownian sliding at the 0.1 ms and 2 ms exposures differ by 1.6 nm, and this is an attainable level of precision for SMID according to Sect. 2.4.3. For the sequence-dependent subdiffusion sliding models, the expected SD difference at the 0.1 ms and 2 ms exposure times would be less than 1.6 nm. Using this difference, we can differentiate Brownian sliding from subdiffusive sliding.

Let us now calculate the expected SD difference between the 0.1 ms and the 2 ms images for the sequence-independent Brownian sliding model. For Brownian diffusions, D_1 is constant in all timescales and the pathway density distribution function $g(x)_{\text{Sliding}}$ is a Gaussian as $g(x)_{\text{Sliding}} \sim \exp(-x^2 / 4D_1t)$, with $2D_1t$ being a reasonable estimate for the variance of $g(x)_{\text{Sliding}}$. Since the convolution of two Gaussians is another Gaussian with variance being the sum of the two variances, the imaged Brownian sliding protein should have a Gaussian intensity profile $I(x)_{\text{Sliding}}$, with $s_{\text{Sliding}}^2 = s_0^2 + 2D_1t$ as

$$I(x)_{\text{Sliding}} \propto \exp(-x^2 / 2(s_0^2 + 2D_1t)). \quad (2.6)$$

Using $\langle D_1 \rangle \approx 10^5 \text{ nm}^2 / \text{s}$ [45], the expected SD difference between $t = 0.1 \text{ ms}$ and $t = 2 \text{ ms}$ is 1.6 nm .

For the 1.6 nm difference to be resolved, the measurement error of each mean SD value at a specific exposure time should be less than one-half of the difference, or 0.8 nm. Assuming each image contains a conservative number of 200 photons (which corresponds to a SD measurement error of 10 nm according to Fig. 2.9), the number of images required for the mean SD error to be less than 0.8 nm is $N_{\text{frames}} \approx 160$ images, according to the relation for error to the mean of $10 \text{ nm} / \sqrt{N_{\text{frames}}} = 0.8 \text{ nm}$.

From the above calculations, if the mean measured SDs increases with t according to $\text{SD}(t) = \sqrt{130^2 \text{ nm}^2 + 2D_1t}$, and differ at 0.1 ms and 2 ms exposure times by $\approx 1.6 \text{ nm}$, then the sliding is Brownian in millisecond timescales. If the mean SDs increase from 0.1 ms to 2 ms slower than $\sqrt{130^2 \text{ nm}^2 + 2D_1t}$, or differ at 0.1 ms and 2 ms exposure times by $< 1.6 \text{ nm}$, then the sliding is subdiffusive.

2.5.3 Will Hopping Be an Issue for the 0.1–2 ms Exposure Times?

During facilitated diffusion, after the first sliding motion, the protein dissociates from DNA and performs a hopping motion. Are the exposure times of 0.1 ms and 2 ms too long such that the protein images may have hopping motions convolved? The

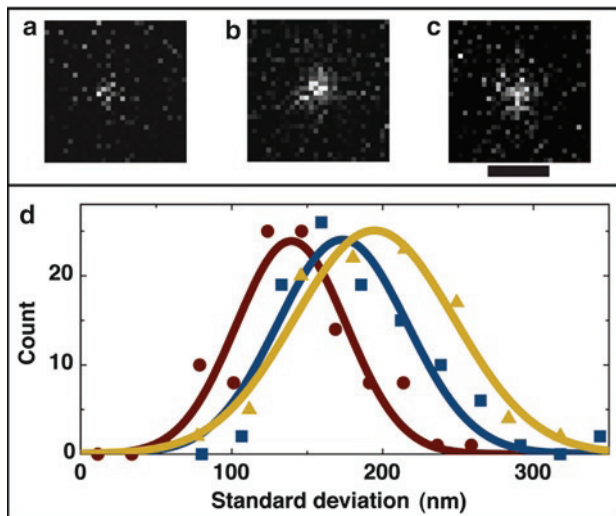


Fig. 2.11 Images of representative single 3D diffusing molecules with exposure times of (a) 0.3 ms, (b) 0.7 ms, and (c) 1 ms. The spread of the molecules increases with exposure time and the SD values are 135 nm (a), 180 nm (b), and 204 nm (c), respectively. (d) SD distributions for exposure times of 0.3 ms (red), 0.7 ms (blue), and 1 ms (yellow). The SD values are 139.5 ± 3.6 nm (mean \pm standard error of the mean), 173.3 ± 4.2 nm, and 194.5 ± 5.2 nm, respectively. The mean of the SD distribution increases with exposure time, indicating that the observed molecules are indeed 3D diffusing molecules. Scale bar, 1 μ m

answer is yes; it is possible that occasionally hopping motion may be convolved in the images. Statistically, if the mean sliding dissociation time is 1 ms, some short slides will inevitably be followed by hopping during exposure and thus some hopping will be convolved in the images. Whether the hopping-convolved images can be differentiated from the purely sliding images will depend on the fraction of time the protein spends hopping during exposure. If the percentage of time for hopping is too high to be ignored, for example, if 1 ms out of a 2 ms exposure is hopping, then the hopping-convolved image will differ dramatically from that of a protein that only moves by sliding. Figure 2.11 shows 3D diffusing molecules with 0.3 ms, 0.7 ms, and 1 ms exposure times and the respective mean SD values of 140 nm, 173 nm, and 195 nm. It is evident that the “blur” of 3D hopping proteins is significantly larger than $s_{\text{sliding}} \approx 130$ nm of the sliding proteins and should be easily discerned if convolved. If the hopping time is short, for example, 0.1 ms out of 2 ms, then the percentage of emitted photons from hopping will be too low to affect the overall SD of the image significantly.

2.5.4 Effect of Defocusing

It is known that the width of a defocused PSF increases [58]. Will defocusing of the sliding proteins affect the expected SD values significantly? Here, we will estimate

the effect using DNA transverse fluctuation analysis. In the transverse and axial directions, a bound-sliding protein should fluctuate the same as the DNA. An elongated λ DNA molecule that extends to the typical 60–90% of its contour length fluctuates transversely with maximum excursion of 100 nm and frequency of 10 Hz (100 ms each cycle, unpublished data). This transverse motion can be approximated to be fluctuation in the axial direction. In the 0.1–2 ms range of exposure times, DNA should have barely moved (or at most defocused by 10 nm) and the defocusing effect on the protein SD should be negligible according to the following relation: the standard deviation $s(\Delta z)$ of a defocused PSF changes with the defocusing distance Δz as [63]

$$s(\Delta z) = s_0 \sqrt{1 + (\Delta z / D)^2}, \quad (2.7)$$

where $D \approx 400$ nm is the depth of field of our imaging system. If we use $z_{Max} = 10$ nm, there is essentially no change to s_0 .

2.5.5 Effect of DNA Longitudinal Fluctuation

Since a protein slides longitudinally along DNA, the longitudinal fluctuation of DNA can introduce blur to the PSF. Here, we estimate the maximum effect DNA longitudinal fluctuation can have on $s_{sliding} = s_x$. According to a simple calculation, the longitudinal displacement of a segment of DNA under tension can be calculated from its measured transverse displacement by assuming that the DNA functions like a spring under tension. For the measured transverse displacement of ± 100 nm at the center of a λ DNA molecule stretched to 10 μm , the corresponding longitudinal displacement at the center segment is $\sqrt{(100 \text{ nm})^2 + (5 \mu\text{m})^2} - 5 \mu\text{m} = 1$ nm. Putting this 1 nm into 6 (in the place of $2D_{\perp}t$), the change to the observed SD should be minimal.

This theoretical estimation awaits experimental validation described in Sect. 2.6.1.2, where the DNA longitudinal fluctuations will be investigated through SD measurements of single specifically bound proteins.

2.6 Prospects for LacI Sliding Studies Using SMID

More experiments and analysis are necessary to unravel the sliding mechanisms of proteins on DNA using SMID. Here, we lay out necessary investigations in detail. We first describe three different, but complementary approaches that should be used in the study: analytical calculations, simulations, and experimental measurements. The intensity profiles of a sliding protein on DNA with exposure times from 0.1 ms to 2 ms should be obtained using each approach and the results should be compared in order to determine the most appropriate mechanism of LacI protein

translocation along nonspecific DNA sequences, or the most appropriate sliding mechanism. If experimental results disagree with the existing translocation models, alternative sliding models should be proposed.

2.6.1 Analytical SD Calculation of Sliding Proteins

In order to obtain analytical expressions for the fluorescence intensity profile and SD of a sliding protein according to the different translocation models, the following studies should be carried out: (1) develop pathway distribution functions $g(x)$ for single trajectories, (2) quantify the effects of defocusing and DNA fluctuation on SD measurements, (3) assess SD measurement error associated with different sliding models, and (4) finally consolidate all analyses to arrive at an expression for expected SD of sliding proteins on DNA for different translocation models.

2.6.1.1 Obtain the Explicit Pathway Distribution Function $g(x)$ for Individual Trajectories

When we calculate the sliding PSF SD value $s_{Sliding}$ in Sect. 2.5.2 using the deconvolution method, the pathway distribution function used was the location distribution at time t for an ensemble of independent trajectories, which is a Gaussian distribution as $g(x) = \exp(-x^2 / 4D_1t)$, where the mean square displacement of many different trajectories at time t is $\langle x^2 \rangle = 2D_1t$. Although it is a good approximation, this $g(x)$ is not exactly appropriate for studying individual trajectories, such as the single sliding proteins we are analyzing. To our knowledge, the pathway distribution function for single Brownian trajectories has not been formulated, in contrast to the well known $P(x) = \exp(-x^2 / 4D_1t)$ relation for an ensemble of independent trajectories.

We have performed preliminary simulations of single Brownian trajectories and observed that the SD of the pathway distribution for single trajectories $s_{SingleTrajectory}$ is at least two times smaller than that of an ensemble of independent trajectories. Additional simulations and analytical calculations are necessary to formulate $s_{SingleTrajectory}$ numerically and analytically.

2.6.1.2 Quantify the Defocusing and DNA Fluctuation Effects Using Single Specifically Bound GFP-LacI Molecules

Although we have estimated in Sects. 2.5.4 and 2.5.5 that the defocusing and DNA fluctuation should have minimal effects on protein sliding measurements, for mechanisms discrimination studies at nanometer precision, the precise effect should be experimentally quantified as an offset to the measured SD.

While the transverse fluctuation of DNA molecules has been extensively investigated [64, 65], the longitudinal fluctuations of elongated DNA molecules have not been studied. Since λ DNA has two *lacO* sites in its sequence, a single LacI can be bound specifically to an elongated λ DNA and the exact $s_{Fluctuation}$ of the protein due to defocusing and DNA fluctuation can be obtained. The DNA molecule will be anchored at both ends onto a fused-silica surface, and the *lacO* sequences between the two anchors can be identified by the specifically bound protein. This study should provide the control measurement for all external effects that may increase the expected SD values of sliding proteins. The difference in SDs between the single specifically bound LacI on DNA and immobile proteins on surfaces will be the SD offset, Δs_{Offset} , resulted from defocusing and DNA longitudinal fluctuation for the experimental setting.

2.6.1.3 Calculate SD Error $\Delta s_{Sliding}$ for Sliding Protein Images

In Sect. 2.4.3, we have developed the SD measurement error expression for immobile single molecules. For mobile molecules, such as sliding proteins on DNA, the SD measurement error should be developed for correct assessment of the measurement precision. Using the new single trajectory pathway distribution functions $g(x)$ for Brownian sliding and subdiffusion slidings to be developed in Sect. 2.6.1.1, the expected intensity profiles of sliding proteins will differ from that of immobile proteins. By using the same method for SD error derivation for immobile single molecules and replacing the intensity profile of the immobile molecules with that of the sliding proteins, SD measurement error for sliding proteins can be obtained [61].

2.6.1.4 SD of the Final Sliding Protein Images

When we combine all factors that may affect the observed $s_{Sliding}$ values, the final theoretical $s_{Sliding}$ should include SD due to the sliding motion $s_{SingleTrajectory}$, the defocusing and DNA fluctuation offset Δs_{Offset} , and SD measurement error $\Delta s_{Sliding}$ as

$$s_{Sliding} = \sqrt{s_{SingleTrajectory}^2 + (\Delta s_{Offset})^2} \pm \Delta s_{Sliding}. \quad (2.8)$$

2.6.2 SD Simulations of Sliding Proteins

In order to simulate the fluorescence intensity profiles of sliding proteins, proteins' trajectories need to convolve with the PSF. All other experimental effects should also be included in the simulation. These effects are DNA fluctuation, defocusing, evanescent light intensity decay, and statistical error originated from fluctuating numbers of photons per PSF, finite camera pixel size, and background noise.

The simulation of sliding LacI images can be carried out in the following order: (1) Simulate 1D Brownian diffusion trajectories along DNA with the known $\langle D_1 \rangle = 10^5 \text{ nm}^2/\text{s}$ and subdiffusion trajectories with a starting b value of 0.5. How do we choose the step size (or time interval for simulation)? This depends on how many photons will be there in an image. If there are 100 photons in a 0.1 ms image, then the step size cannot be smaller than the interval during which one photon is detected, or $0.1 \text{ ms}/100 = 1 \mu\text{s}$. (2) Incorporate the transverse and axial direction fluctuations into the 1D trajectories according to DNA's transverse fluctuations, thus forming a 3D trajectory. (3) At each step, insert a PSF. The PSF should only have one photon, and the location of the photon will be randomly distributed within the PSF according to the PSF Gaussian photon distribution. The PSF SD will change according to the axial location 7. (4) Correct each photon count by a weighting factor, since the decaying evanescent excitation (Fig. 2.3b) does not excite the fluorophore at all depths equally. (5) Bin the simulated weighted photons for the whole image into pixels to include the camera pixelation effect. (6) Add the background noise to the binned image. (7) Fit the final intensity profile to a 2D Gaussian to obtain the SD value for the image. (8) Obtain the SD distribution for many simulated images for a specific exposure time. (9) Add the DNA fluctuation and defocusing offset s_{Offset} to the mean SD. (10) Plot and compare the mean SD values at different exposure times with experimental data.

2.6.3 *Experimental SD Measurements of Sliding LacI on λ DNA*

In Sect. 2.5.1, SD distributions of diffusion LacI on DNA were measured for three exposure times of 5 ms, 10 ms, and 15 ms. Although changes in SD with exposure time are apparent, these exposure times might be too long for hopping to be negligible. In order to ensure detection of genuine sliding motion, exposure times of 0.1–2 ms should be used.

The mean SD values from SD distributions at various exposure times should be plotted. If SDs increase with t as $\text{SD}(t) = \sqrt{s_0^2 + CD_1 t}$, where C is the coefficient for single trajectories that will be calculated in Sect. 2.6.1.1, the sliding is Brownian. If the SD increases are less, then the sliding is subdiffusive.

2.6.4 *Resolution Limits, Alternative Translocation Models, and Extensions*

During experiments, the following items might be of concern and may introduce further complications to the studies.

2.6.4.1 Resolution Limitation

It is possible that even with nanometer resolution of the SD measurements, different sliding models may not be differentiated if the SD difference between the models is less than the SD measurement error, which in our case is ≈ 0.8 nm (Sect. 2.5.2). One example is the DNA-sequence-dependent sliding Models I and III (Fig. 2.7), where their $\langle n^2 \rangle$ values at 2 ms are almost identical. If this occurs, then this study can at least rule out subdiffusion models with a b value significantly lower than 0.5, or models with a very low A or D_1 value, or the combination of the three.

2.6.4.2 Obtain the Realistic Sliding–Hopping Alternation Kinetics by Simulation

In spite of recent experimental and theoretical investigations of protein hopping on DNA [30, 66], the real hopping interval distribution and nonspecific DNA dissociation time distribution remain unclear. Simulation might offer a solution to the problem. The whole sliding and hopping process to seconds long can be simulated using Brownian dynamics to search for a combination of sliding characteristics and hopping time distribution that yield the known LacI 1D Brownian diffusion with $\langle D_1 \rangle = 10^5 \text{ nm}^2 / \text{s}$ in the timescale of seconds [45]. The results should provide validation for the interpretation of experimental results.

2.6.4.3 Uncertain Sliding Dissociation Time and Possible Alternative Sliding Model

If the unknown sliding time is more than 5 ms, the lowest exposure time used in experiments in Sect. 2.5.1, then reinterpretation of data in Fig. 2.10 for the 5-ms exposure time suggests an alternative mechanism of translocation: one that diffuses fast on millisecond timescales and slow on second timescales.

Let us calculate the expected SD (s_{sliding}) for the Brownian sliding model assuming that the mean sliding time is longer than 5 ms. Since the sliding is Brownian for all timescales, D_1 is constant at all timescales. Putting the experimental values of $t = 5$ ms and $\langle D_1 \rangle = 10^5 \text{ nm}^2/\text{s}$ [45] into 6, $s_{\text{sliding}} = 133.7$ nm. This calculated s_{sliding} is significantly lower than the measured mean value of $\langle S_x \rangle = 165 \pm 2.6$ nm (Fig. 2.10b). This result suggests faster diffusion in millisecond timescales than in second timescales, contradicting the existing Brownian sliding and subdiffusion sliding models.

2.6.5 Relating Physical and Biological Significance

In some respects, the *rate* at which transcription factors find their specific sites is not a very interesting biological problem. While you can worry about the speed

needed to find transcription factor sites in rapidly growing cells such as *E. coli*, for some cells there would seem to be plenty of time for the proteins to find their sites given the known range of on and off nonspecific dissociation dynamics and the probable size of the specific site at which the transcription factor binds tightly. It is possible that a far more important biological problem is as follows: what is the physics of how tight association to a specific sequence of basepairs occurs as opposed to the secondary issue of how the site is found.

The common thread linking the specific and nonspecific binding is the DNA sequence, just as in the protein problem the common thread linking folding rates and activity is the amino acid sequence. In this paper, we discuss a new way to analyze the dynamics of transcription factor dynamics on a DNA molecule in terms of pathway distribution function $g(x)$, the position-(and time) dependent dynamics of the transcription factor moving along the DNA molecule. It is somewhat comparable to the distribution of conformation states $g(E)$ that the Frauenfelder group developed some years ago which characterized the probability distribution of a protein on a free energy landscape and the subsequent dynamics [39, 67]. We can ask if, perhaps, the $g(x)$ we introduce here could play a similar role for the movement of a transcription factor along the DNA as it moves in a, perhaps, sequence-directed manner toward deep specific binding sites. This approach could elucidate the basic biologically relevant mechanisms.

2.7 Summary

In this chapter, we present single-molecule fluorescence imaging studies of LacI protein diffusing along elongated DNA molecules and detail the studies necessary to discriminate different sliding mechanisms of proteins on DNA using theoretical calculations, simulations, and experimental measurements. A new method, SMID, that can improve the temporal resolution of single-molecule tracking experiments by 100-fold is developed and applied to LacI diffusion studies. The experimental and analytical methods presented here should advance the single-molecule imaging field by providing a new method that improves the temporal and spatial resolutions of single-molecule tracking. The sliding mechanism research should provide fundamental insights into how proteins interact with nonspecific DNA sequences and help to quantify the effect of facilitated diffusion on gene regulation.

References

1. Ptashne M (1992) A genetic switch: phage lambda and higher organisms, 2nd edn. Blackwell, Cambridge, MA
2. Alberts B, Johnson A, Lewis J, Raff M, Roberts K, Walter P (2002) Molecular biology of the cell, fourth edn. Garland Science, New York

3. Revzin A (1990) The biology of nonspecific DNA protein interactions. CRC Press, London
4. Riggs AD, Bougeois S, Cohn M (1970) The *lac* repressor-operator interaction. 3. Kinetic studies. *J Mol Biol* 53:401–417
5. Adam G, Delbruck M (1968) Reduction of dimensionality in biological diffusion process. In: Rich A, Davidson N (eds) Structural chemistry in molecular biology, Freeman, San Francisco, pp. 198–215
6. Berg OG, Blomberg C (1976) Association kinetics with coupled diffusional flow. Special application to the Lac repressor-operator system. *Biophys Chem* 4:367–381
7. Berg OG (1978) On diffusion-controlled dissociation. *Chem Phys* 31:47–57
8. Winter RB, von Hippel PH (1981) Diffusion-driven mechanisms of protein translocation on nucleic acids. 2. The *Escherichia coli* repressor-operator interaction: equilibrium measurements. *Biochemistry* 20:6948–6960
9. Jack WE, Terry BJ, Modrich P (1982) Involvement of outside DNA sequences in the major kinetic path by which EcoRI endonuclease locates and leaves its recognition sequence. *Proc Natl Acad Sci U S A* 79:4010–4014
10. Ricchetti M, Metzger W, Heumann H (1988) One-dimensional diffusion of *Escherichia coli* DNA-dependent RNA polymerase: A mechanism to facilitate promoter location. *Proc Natl Acad Sci U S A* 85:4610–4614
11. Ruusala T, Crothers DM (1992) Sliding and intermolecular transfer of the Lac repressor - kinetic perturbation of a reaction intermediate by a distant DNA-sequence. *Proc Natl Acad Sci U S A* 89:4903–4907
12. Kabata H, Kurosawa O, Arai I, Washizu M, Margaron SA, Glass RE, Shimamoto N (1993) Visualization of single molecules of RNA polymerase sliding along DNA. *Science* 262:1561–1563
13. Hsien M, Brenowitz M (1997) Comparison of the DNA association kinetics of the Lac repressor tetramer, its dimeric mutant LacI^{adj} and the native dimeric Gal repressor. *J Biol Chem* 272:22092–22096
14. Shimamoto N (1999) One-dimensional diffusion of proteins along DNA. *J Biol Chem* 274:15293–15296
15. Halford SE, Marko JF (2004) How do site-specific DNA-binding proteins find their targets? *Nucleic Acids Res* 32:3040–3052
16. Misteli T (2001) Nuclear structure - Protein dynamics: Implications for nuclear architecture and gene expression. *Science* 291:843–847
17. Stanford NP, Szczelkun D, Marko JF, Halford SE (2000) One- and three-dimensional pathways for proteins to reach specific DNA sites. *EMBO J* 23:6546–6557
18. Gowers DM, Halford SE (2003) Protein motion from non-specific to specific DNA by three-dimensional routes aided by supercoiling. *Embo J* 22:1410–1418
19. Elf J, Li G-W, Xie XS (2007) Probing transcription factor dynamics at the single-molecule level in a living cell. *Science* 316:1191–1194
20. Biebricher A, Wende W, Escudé C, Pingoud A, Desbiolles P (2009) Tracking of single quantum dot labeled EcoRV sliding along DNA manipulated by double optical tweezers. *Biophys J: Biophys Lett* 96:L50–L52
21. Li G-W, Berg OG, Elf J (2009) Effects of macromolecular crowding and DNA looping on gene regulation kinetics. *Nat Phys* 5:294–297
22. Barbi M, Place C, Popkov V, Salerno M (2004) A model of sequence-dependent protein diffusion along DNA. *J Biol phys* 30:203–226
23. Berg OG, Ehrenberg M (1982) Association kinetics with coupled three- and one-dimensional diffusion : Chain-length dependence of the association rate to specific DNA sites. *Biophys Chem* 15:41–51
24. Gowers DM, Wilson GG, Halford SE (2005) Measurement of the contributions of 1D and 3D pathways to the translocation of a protein along DNA. *Proc Natl Acad Sci U S A* 102:15883–15888
25. Porecha RH, Stivers JT (2008) Uracil DNA glycosylase uses DNA hopping and short-range sliding to trap extrahelical uracils. *Proc Natl Acad Sci U S A* 105:10791–10796

26. Harada Y, Funatsu T, Murakami K, Nonoyama Y, Ishihama A, Yanagida T (1999) Single-molecule imaging of RNA polymerase-DNA interactions in real time. *Biophys J* 76:709–715
27. Berg OG, von Hippel PH (1985) Diffusion-controlled macromolecular interactions. *Annu Rev Biophys Chem* 14:131–160
28. Barkley MD (1981) Salt dependence of the kinetics of the *lac* repressor-operator interaction: role of nonoperator deoxyribonucleic acid (DNA) in the association reaction. *Biochemistry* 20:3833–3842
29. Hu L, Grosberg AY, Bruinsma R (2008) Are DNA transcription factor proteins Maxwellian demons? *Biophys J* 95:1151–1156
30. Wunderlich Z, Mirny LA (2008) Spatial effects on the speed and reliability of protein-DNA search. *Nucleic Acids Res* 36:3570–3578
31. Wang YM, Tegenfeldt J, Reisner W, Riehn R, Guan X-J, Guo L, Golding I, Cox EC, Sturm J, Austin RH (2005) Single-molecule studies of repressor-DNA interactions show long-range interactions. *Proc Natl Acad Sci U S A* 102:9796–9801
32. Perkins TT, Smith DE, Larson RG, Chu S (1995) Stretching of a single tethered polymer in a uniform flow. *Science* 268:83–87
33. Kalodimos CG, Biris N, Bonvin AMJJ, Levandoski MM, Guennegues M, Boelens R, Kaptein R (2004) Adaptation in nonspecific and specific protein-DNA complexes. *Science* 305:386–389
34. Smith SB, Finzi L, Bustamante C (1992) Direct mechanical measurements of the elasticity of single DNA molecules by using magnetic beads. *Science* 258:1122–1126
35. Thompson RE, Larson DR, Webb WW (2002) Precise nanometer localization analysis for individual fluorescent probes. *Biophys J* 82:2775–2783
36. Qian H, Sheetz MP, Elson EL (1991) Single particle tracking: Analysis of diffusion and flow in two-dimensional systems. *Biophys J* 60:910–921
37. Blainey PC, van Oijent AM, Banerjee A, Verdine GL, Xie XS (2006) A base-excision DNA-repair protein finds intrahelical lesion bases by fast sliding in contact with DNA. *Proc Natl Acad Sci U S A* 103:5752–5757
38. Graneli A, Yeykal C, Robertson R, Greene E (2006) Long-distance lateral diffusion of human Rad51 on double-stranded DNA. *Proc Natl Acad Sci U S A* 103:1221–1226
39. Austin RH, Beeson K, Eisenstein L, Frauenfelder H, Gunsalus I, Marshall V (1974) Activation energy spectrum of a biomolecule: Photodissociation of carbonmonoxy myoglobin at low temperatures. *Phys Rev Lett* 32:403–405
40. Slutsky M, Mirny LA (2004) Kinetics of protein-DNA interaction: Facilitated target location in sequence-dependent potential. *Biophys J* 87:4021–4035
41. Barbi M, Place C, Popkov V, Salerno M (2004) Base-sequence-dependent sliding of proteins on DNA. *Phys Rev E* 70:041901
42. Gerland U, Moroz JD, Hwa T (2002) Physical constraints and functional characteristics of transcription factor–DNA interaction. *Proc Natl Acad Sci U S A* 99:12015–12020
43. Berg OG, von Hippel PH (1989) Selection of DNA binding sites by regulatory proteins statistical-mechanical theory and application to operators and Promoters. *J Mol Biol* 193:723–750
44. von Hippel P, Rees WA, Rippe K, Wilson KS (1996) Specificity mechanisms in the control of transcription. *Biophys Chem* 59:231
45. Wang YM, Austin RH, Cox EC (2006) Single molecule measurements of repressor protein 1D diffusion on DNA. *Phys Rev Lett* 97:048302
46. Gorman J, Chowdhury A, Surtees JA, Shimada J, Reichman DR, Alani E, Greene EC (2007) Dynamic Basis for one-dimensional DNA scanning by the mismatch repair complex Msh2-Msh6. *Cell* 28:359–370
47. Kim JH, Larson RG (2007) Single-molecule analysis of 1D diffusion and transcription elongation of T7 RNA polymerase along individual stretched DNA molecules. *Nucleic Acids Res* 35:3848–3858
48. Tafvizi A, Huang F, Leith JS, Fersht AR, Mirny LA, van Oijen AM (2008) Tumor Suppressor p53 Slides on DNA with low friction and high stability. *Biophys J: Biophys Lett* 95:L01–L03

49. Bonnet I, Biebricher A, Porté P-L, Loverdo C, Bénichou O, Voituriez R, Escudé C, Wende W, Pingoud A, Desbiolles P (2008) Sliding and jumping of single EcoRV restriction enzymes on non-cognate DNA. *Nucleic Acids Res* 36:4118–4127
50. Gorman J, Greene EC (2008) Visualizing one-dimensional diffusion of proteins along DNA. *Nat Struct Mol Biol* 15:768–774
51. van Mameren J, Peterman EJG, Wuite GJL (2008) See me, feel me: methods to concurrently visualize and manipulate single DNA molecules and associated proteins. *Nucleic Acids Res* 36:4381–4389
52. Komazin-Meredith G, Mirchev R, Golan DE, van Oijen AM, Coen DM (2008) Hopping of a precessivity factor on DNA revealed by single-molecule assays of diffusion. *Proc Natl Acad Sci U S A* 105:10721–10726
53. Laurence TA, Kwon Y, Johnson A, Hollars CW, O'Donnell M, Camarero JA, Barsky D (2009) Motion of a DNA sliding clamp observed by single molecule fluorescence spectroscopy. *J Biol Chem* 283:22895–22906
54. Lin Y, Zhao T, Jian X, Farooqui Z, Qu X, He C, Dinner AR, Scherer NF (2009) Using the bias from flow to elucidate single DNA repair protein sliding and interactions with DNA. *Biophys J* 96:1911–1917
55. Kurita H, Torii K, Yasuda H, Takashima K, Katsura S, Mizuno A (2009) The effect of physical form of DNA on exonuclease III activity revealed by single-molecule observations. *J Fluoresc* 19:33–40
56. Fan H-F, Li H-W (2009) Studying RecBCD helicase translocation along χ -DNA using tethered partial motion with a stretching force. *Biophys J* 96:1875–1883
57. van Oijen A, Köhler J, Schmidt J, Müller M, Brakenhoff G (1998) 3-Dimensional super-resolution by spectrally selective imaging. *Chem Phys Lett* 292:183–187
58. Speidel M, Jonas A, Florin E-L (2003) Three-dimensional tracking of fluorescent nanoparticles with subnanometer precision by use of off-focus imaging. *Opt Lett* 28:69–71
59. Huang B, Wang W, Bates M, Zhuang X (2008) Three-dimensional super-resolution imaging by stochastic optical reconstruction microscopy. *Science* 319:810–813
60. DeCenzo S, DeSantis M, Wang YM (2010) Single-image separation measurements of two unresolved fluorophores. *Opt Express* 18:16628–16639
61. DeSantis M, DeCenzo S, Li JL, Wang Y (submitted) Precision analysis for standard deviation measurements of immobile single fluorescent molecule images. *Opt Express* 18:6563–6576
62. Yildiz A, Tomishige M, Vale RD, Selvin PR (2004) Kinesin walks hand-over-hand. *Science* 303:676–678
63. Schütz GJ, Pastushenko VP, Gruber HJ, Knaus H-G, Pragl B, Schindler H (2000) 3D imaging of individual ion channels in live cells at 40 nm resolution. *Single Mol* 1:25–31
64. Quake SR, Babcock H, Chu S (1997) The dynamics of partially extended single molecules of DNA. *Nature* 388:151–154
65. Crut A, Lasne D, Allemand JF, Dahan M, Desbiolles P (2003) Transverse fluctuations of single DNA molecules attached at both extremities to a surface. *Phys Rev E* 67:051910
66. Loverdo C, Bénichou O, Voituriez R (2009) Quantifying hopping and jumping in facilitated diffusion of DNA-binding proteins. *Phys Rev Lett* 102:188101
67. Austin R, Beeson K, Eisenstein L, Frauenfelder H, Gunsalus I, Marshall V (1975) Dynamics of ligand binding to myoglobin. *Biochemistry* 14:5355–5373

Biophysics of DNA-Protein Interactions
From Single Molecules to Biological Systems

Williams, M.C.; Maher, III, L.J. (Eds.)

2011, X, 350 p., Hardcover

ISBN: 978-0-387-92807-4